Crystal structure of tetrachloride ferrate (III) complex with methylene blue

VAHOBJON KH. SABIROV

Pharmaceutical Institute of Education and Researches, 100114,
Tashkent, Yunusabad district, 19 quarter, 46 building, UZBEKISTAN

Abstract: Crystal structure of tetrachloride ferrate (III) complex of methylene blue, $[MB]^+[FeCl_4]^-$ (where $[MB]^+$ methylthioninium or 3,7-bis(dimethylamino)-phenothiazine-5-ium cation), has been prepared by mechanochemical way and studied by the single crystal X-ray crystallography. The crystal structure of title compound is built from by $[FeCl_4]^{2-}$ tetrahedral ion and planar $[MB]^+$ counter ions. The $[MB]^+$ cations stacked in an antiparallel fashion with the sulfur atom disposed alternatively on an opposite sides. A dihedral angle between planes of the two adjacent MB^+ cations equal to 2.6(1)°. The centroid–centroid distances between stacked MB^+ cations vary in the range of 3.609 (2) and 3.802 (2) Å. The $[MB]^+$ cations are connected in the 3D network by the C–H···Cl hydrogen bonds. Details of short contacts were analyzed by 3D Hirshfeld surfaces and 2D fingerprint plots. Intermolecular interaction energy between two adjacent MB+ cations was calculated using two CE-B3LYP/6-31G (d,p) theoretical level.

Keywords: ferrate (III); methylene blue; π-π stacking; Hirschfeld surfaces.
Received: January 14, 2023. Revised: October 15, 2023. Accepted: November 19, 20223. Published: December 29, 2023.

1. Introduction

The current high interest in methylene blue is explained by its wide using in medical purposes [1]. It shows the positive effect in the treatment of Alzheimer's disease (AD) [2], methemoglobinemia and COVID–19 [3]. It is an effective antidote for due to its own oxidizing properties [4].

Methylene blue or 3,7-bis(dimethylamino)phenothiazin-5-ium cation, $[MB]^+$ - methylthioninium cation, consists of three condensed six-membered rings and two exocyclic coplanar NMe_2 substituents (Fig. 1). The $[MB]^+$ cation can be described in the predominant resonance structures **I, II** and **III**: **I** with the formal charge localized on the S atom, **II** and **III** with the formal charge localized on exocyclic N atoms [5].

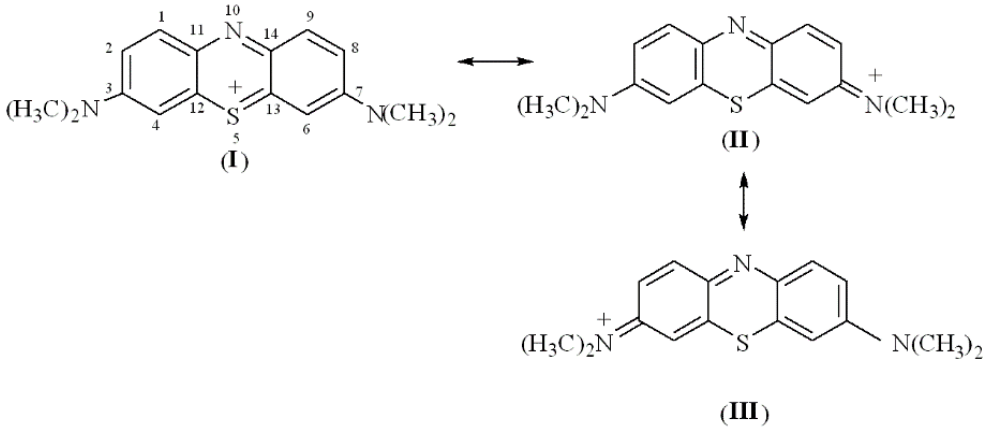

Figure 1. Resonance forms of the $[MB]^+$ cation with numbering of atoms.

The $[MB]^+$ has N and S atoms in the central ring as possible electronic donor atoms. The eventual coordination of $[MB]^+$ to soft acids, such as Hg^{2+} and Ag^+, is expected to happen through the S atom and not the N atoms, according to Pearson hard and soft acid and base theory [6]. However, this is not observed experimentally and coordination of $[MB]^+$ through the N atom of the central ring was observed only in the complexes of the Cu(I) chloride with $[MB]^+$ [7, 8]. In the complexes of the Hg(II) [5], the different types of coordination ability of the $[MB]^+$ cation is shown.

Our investigations are motivated by searching for the new medicines against AD and other diseases on the bases of the complexes *d*-metals with MB. Given paper discuss the synthesis and single X-ray diffraction study of the ferrate complex of MB, [MB][FeCl4], reared during the mechanochemical synthesis. The intermolecular interaction energies were calculated between adjacent MB^+ cations.

2. Materials, Experimental, and Theoretical Methods

2.1. Synthesis

Complex $[MB][FeCl_4]$ was prepared from the $FeCl_4{\cdot}6H_2O$ salt and $[MB]Cl{\cdot}5H_2O$ by using mechanochemical synthesis. The $FeCl_3{\cdot}6H_2O$ salt (41.10 mg, 0.152 mmol) and $[MB]Cl{\cdot}5H_2O$ (50 mg, 0.152 mmol) were ground in an agate mortar until a gold-like thin mass on the down of the mortar was formed. 5.0 ml of DMF was gradually added dropwise to the reaction mixture and grounding was continued until a homogeneous dark blue at the mortar was appeared. Crystals available for X-ray data collection were obtained by evaporation of the reaction solution in the thermostat at 40°C.

2.2. XRD analysis

All X-ray diffraction experiments were carried out on an 'XtaLAB Synergy, HyPix3000' difractometer (Cu$K\alpha$ radiation, λ = 1.54184 Å, ω-scan mode, mirror monochromator) at T = 293 K [9]. Crystal data, data collection and structure refinement details are summarized in Table 1. The crystal structure of **1** were solved on Olex2 [[10] using the SHELXT program [11], and refined (full-matrix least-squares refinement on F^2) using the SHELXL program refinement package using least squares minimization [12]. All non-hydrogen atoms were refined anisotropically. The H atoms of the CH_3 – groups were included in calculated positions and refined as riding: C–H = 0.95–0.98 Å with U_{iso}(H) = 1.5U_{eq}(C-methyl) and 1.2U_{eq}(C) for other H atoms.

The molecular drawings were plotted by MERCURY program package [13]. Using the software Platon [14, 15], water molecules crystallization, the hydrogen bonds and short non-bonded contacts were analyzed. The data collection, crystal parameters and refinement details of (1) and (2) are shown in Table 1. Crystallographic data have been deposited with Cambridge Crystallographic Data Centre (Deposite Number xxxx). The data can be obtained free of charge via http://www.ccdc.cam.ac.uk/conts/ retrieving.html or from the Cambridge Crystallographic Data Centre, 12 Union Road, Cambridge CB2 1EZ, UK; fax: (+ 44) 1223-336-033; or e-mail: deposit@ccdc.cam.ac.uk.

Table 1. Crystal data and structure refinement parameters for **I**.

Empirical formula	$C_{16}H_{18}N_3Cl_4SFe$
Formula weight	482.063
Temperature/K	293
Crystal system	monoclinic
Space group	$P2_1/c$
a, Å	15.0077(5)
b, Å	17.4746(6)
c, Å	7.9490(4)
α, °	90

β, °	92.572(4)
γ, °	90
Volume/Å^3	2082.55(14)
Z	4
$\rho_{calc,}$ g·cm^{-3}	1.538
μ/mm^{-1}	11.505
F(000)	985.2
Crystal size/mm^3	0.3 × 0.2 × 0.3
Radiation	Cu K_α (λ = 1.54184)
2Θ range for data collection/°	5.9 to 143.14
Index ranges	-17 ≤ h ≤ 18, -21 ≤ k ≤ 21, -9 ≤ l ≤ 9
Reflections collected	21130
Independent reflections	4037 [R_{int} = 0.0946, R_{sigma} = 0.0707]
Data/restraints/parameters	4037/0/231
Goodness-of-fit on F^2	0.995
Final R indexes [I>=2σ (I)]	R_1 = 0.0554, wR_2 = 0.1329
Final R indexes [all data]	R_1 = 0.1006, wR_2 = 0.1617
Largest diff. peak/hole / e Å^{-3}	0.42/-0.46

2.3. Theoretical Methods

Intermolecular interactions were analyzed by using the CrystalExplorer17 program [16 - 18]. 3D-Hirshfeld surface (HS) calculations were calculated over the d_{norm} in the range of -0.1620 (red) to 1.2993 (blue) Å, shape index in the range of 1.000 to 1.000 Å and curvedness range are in the range -4.000 to 0.4000 Å. The 2D-fingerprint plots were calculated by using the standard 0.6-2.6 Å view with the d_e and d_i distance scales displayed on the graph axes. The intermolecular interaction energies were calculated using the CE-B3LYP/6–31+G (d, p) theoretical level.

3. Results and Discussion

3.1. Description of the crystal structure

The crystal structure of [MB][$FeCl_4$] (**1**) is built from the [$FeCl_4$]$^{2-}$ ion and one [MB]$^+$ counter ions (Fig.2). The [$FeCl_4$]$^-$ ion is practically a regular tetrahedron. The Fe–Cl distances vary in a range of 2.246(1) – 2.299(1) Å, the Cl–Fu–Cl bond angles are in the range of 105.8(1)-113.2(1)^o (Table 1). The [MB]$^+$ cations are planar: the C32–N3–C3–C4 and C72–N7–C7–C4 torsion angles are 0 and 2°, respectively.

Figure 2. An asymmetric unit of complex (1).

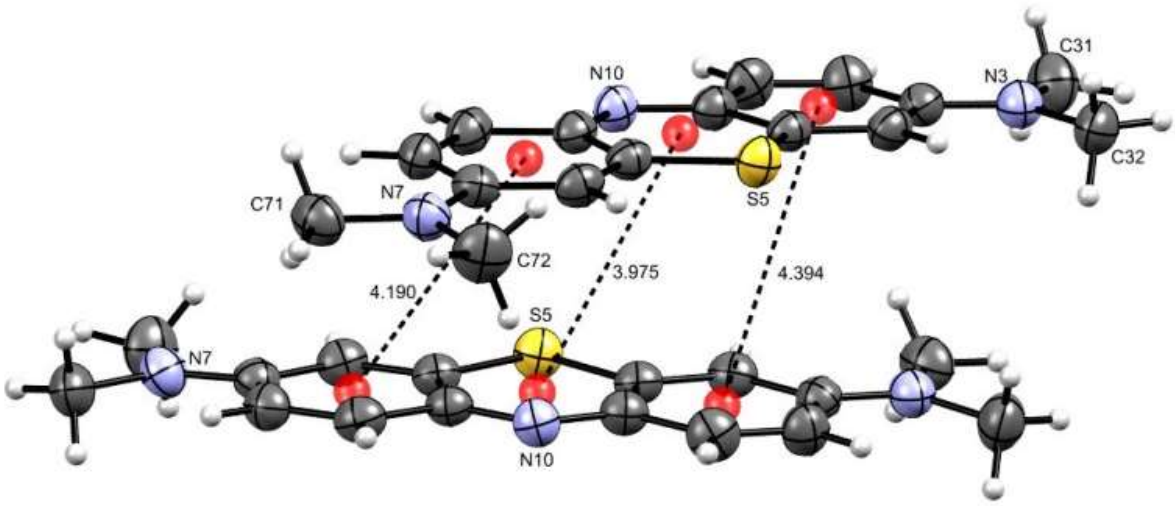

Figure 3. Mutual arrangement of the $[MB]^+$ cations in the stacking and the intercentroid distances between aromatic rings.

In the crystal structure **1**, as it meets in the other compounds of MB [7, 8, 19-22], the $[MB]^+$ cations are packed in the antiparallel π-π stacks with the sulfur atoms disposed alternatively on opposite sides. The planes of thr between aromatic rings of the adjacent $[MB]^+$ cations are almost parallel: the angle between planes is of 2.5°.

An angle between principal molecular axes of the adjacent MB^+ cations is ~36°. The average interplanar distance is 3.531(6) Å. However, the intercentroid distances between adjacent $[MB]^+$ cations vary in the range of 4.190(6) – 4.394(6) Å (**Fig. 3**).

Both S–C bonds in the central ring are similar in lengths (1.728 (5) and 1.729 (5) Å). The N10–C11 and N10–C14 bond lengths are equivalent (1.331(5) and 1.333(6) Å). The N3–C3 and N7–C7 side bonds are different: 1.354 (6) and 1.367 (6) Å, respectively. These geometrical parameters of the $[MB]^+$ cation correspond to the predominant resonance forms of the $[MB]^+$ cation **II** either **III**.

The $[MB]^+$ cations located in the adjacent parallel planes cross-linked through a weak bond C-H···C and the C-H···Cl hydrogen bonds involving the $[FeCl_4]^-$ ion in the 3D-network (Fig.4, Table 3). The displacement of the $[MB]^+$ cations in adjacent stacks leads to the formation of a zigzag chains along axis ***c***.

Each $[MB]^+$ cation forms the short intermolecular contacts C–H···Cl with five adjacent $[FeCl_4]^-$ anions (Fig. 3). There is a weak interaction C32–H···C3 between two cations: where the distances C32···C3 and H···C3 are 3.559 Å and 2.8 Å, respectively and angle ∠C32-H···C is 138° The geometry of all the short contacts mentioned here is presented in Table 2.

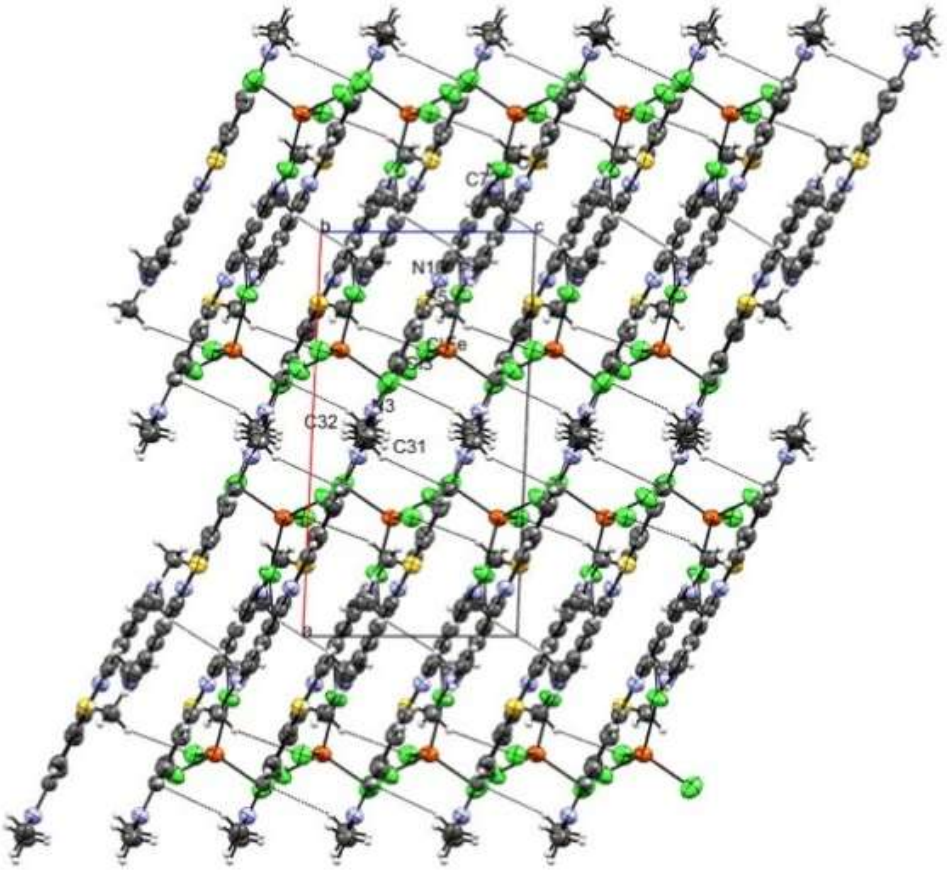

Figure 4. A packing diagram of the title compound, viewed along the *c* axis, showing the short contacts as dashed lines.

Table 2. Geometry of the short intermolecular contacts.

D—H···A	D—H	H···A	D···A	D—H···A
C2—H2···Cl4^{i}	0.93	2.74	3.580(5)	150
C71—H71A···Cl1^{ii}	0.93	2.78	3.673(6)	156
C9—H9···Cl2^{iii}	0.93	2.94	3.745(6)	146
C6—H6···Cl2^{iv}	0.93	2.88	3.723(6)	152
C31—H31B···Cl1^{v}	0.96	2.98	3.907(6)	162
C32—H32A···C3^{v}	0.96	2.79	3.559(8)	137

Symmetry codes: (i) $-x+1, y-1/2, -z+1/2$; (ii) $x-1, y, z$; (iii) $x-1, -y-1/2, z+1/2$; (iv) $-x+1, -y+1, -z+1$; (v) $x, -y+1/2, z-1/2$.

3.2. Database survey

The Cambridge Structural Database [23] (Groom *et al.*, 2016) includes 11 salts and 13 metal complexes of $[MB]^+$ [18]. In the complexes of the Cu(I) and Ag(I) with ref-codes YAYCEJ and YAYCIN, respectively, the metal ions are coordinated by the $[MB]^+$ cation through the N atom of the phenothiazine ring. In the complexes of the $Hg(II)Cl_2$, the salt type complex $[MB]^+_2[HgCl_4]^-_2$ is obtained [Raj *et al.*, 2007]. In the crystal structure of the $[MB](NO_3)\cdot 2H_2O$ salt (Kavita *et al.*, 2004), the interlanar distance is 3.7040 (18) A (IZAJIC). In other compounds, it acts as a counterion.

4. Theoretical study

4.1. 3D and 2D Hirshfeld surface calculations.

Any types of the intra- or intermolecular interactions can be visualized by using Hirshfeld surface analysis of the structure. The red spots over the Hirshfeld surfaces on the d_{norm} surface arise as a result of the short interatomic contacts, while the other intermolecular interactions appear as light-red spots (Fig. 5*a*). The blue area represents completely free from close contacts. The red spot on that surface indicate the C–H···Cl hydrogen bond between $[MB]^+$ cation and $[FeCl_4]^-$ anion, and lighter red spot specify the C32–H•••C3 (*x*, -*y*+1/2, *z*-1/2) interaction between two $[MB]^+$ cations. The relatively bright red spots on d_e map clearly displays the atoms of the MB^+ cation taking participation on the short contacts. In the title compound, no classical hydrogen bonds are present.

On the shape index, convex blue spot located around the azomethyl group represent hydrogen donor groups and concave red regions represent hydrogen acceptor groups (5*b*).

The Hirshfeld surface analysis also shown that π···π stacking interactions between the adjacent MB^+ cations exist, as can be inferred from inspection of the neighboring red and blue triangles (highlighted by yellow circles) on the shape-index surface. This type of stacking interaction appears as a flat region on the curvedness and on the shape-index as red and blue triangles on the aromatic rings. Indeed, the pattern of red and blue triangles in the same region of the shape-index surface is characteristic of π-π stacking interactions; the blue triangles represent convex regions resulting from the presence of ring carbon atoms of the molecule inside the surface, while the red triangles represent concave regions caused by carbon atoms of the π-π stacked molecule above.

The shape of the blue outline on the curvedness surface unambiguously delineates the contacting patches of the molecules. The nearest neighbor coordination environment of the molecules is identified from the color patches on the Hirshfeld surface based on their closeness to adjacent molecules. Therefore, the fragment patches show the appropriate approach for the identification of the nearest neighboring coordination environment of the $[MB]^+$ cation.

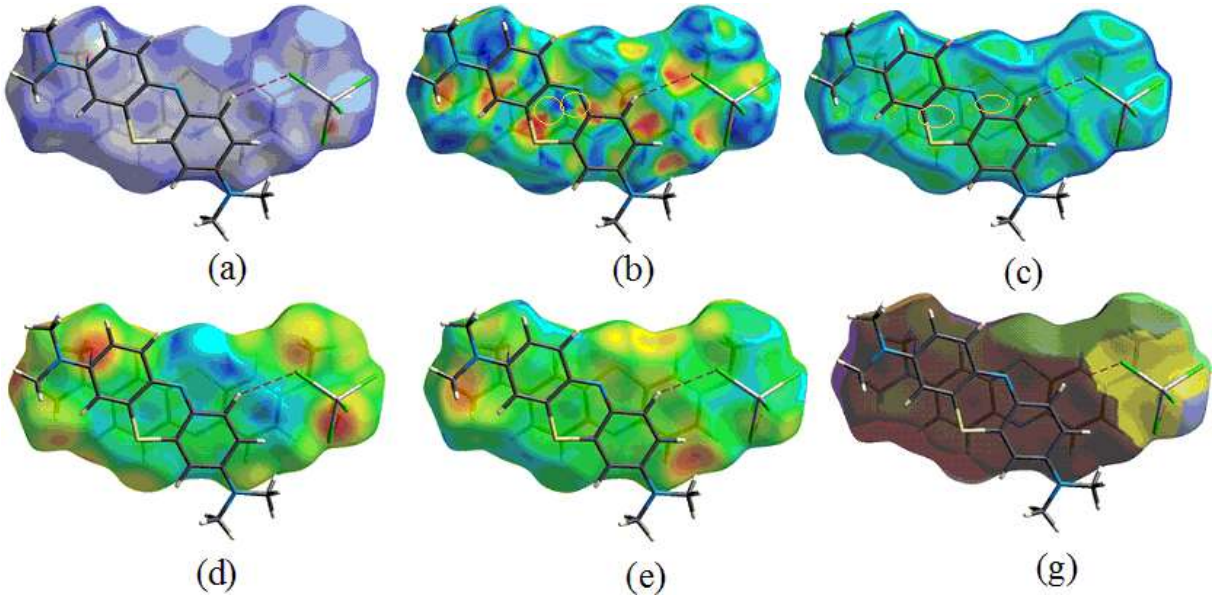

Figure 5. The Hirshfeld surfaces for crystal **I:** (a) mapped over d_{norm} , (*b*) shape index, (*c*) curvedness, (*d*) d_e , (*e*) d_i and (*g*) fragment patch surface.

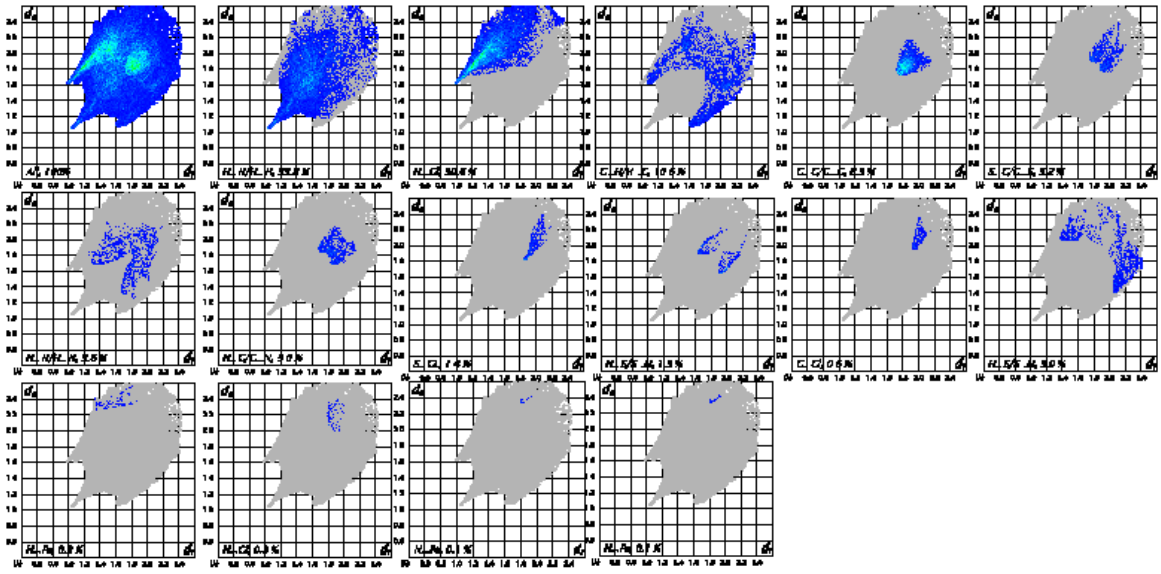

Figure 6. 2D fingerprint plots with the relative contributions to the Hirshfeld surface.

The 2D fingerplots show the contributions of the different intermolecular contacts to total Hirshfeld surface. As shown in the Fig. 6, a large contribution to the total intermolecular interaction was made by the H···H contacts with 33.8 %. The H···Cl and C···H/H···C interactions were the second and third major interactions, and they contributed to the total Hirshfeld surface by approximately 30.1 % and 10.6 %, respectively. The C···C contacts corresponding to the π–π interaction of two neighbor $[MB]^+$ cations made contribution 8.3 %. The small contribution of C···C contacts is explained by a large shift of the aromatic rings of neighboring $[MB]^+$ cations (large distances between centroids) relative to each to other and their small overlap. The contributions from other contacts negligible effects on the packing.

4.2. Intermolecular interaction energy calculations

Obviously, intermolecular interaction or association energy of MB^+ cation is helpful in understanding its dimerization and polymerization in water solution and crystals, as well as for the construction of polylayer structures on the surface of the solids for the application it in photosensibilator production and design of new drugs.

The pairwise intermolecular interaction energies were calculated for two adjacent [MB]+ cations in the π···π stacking by using CE-B3LYP [18] program on a basis set of 6– 31+G(d,p) with the charges +1 and -1 for $[MB]^+$ cation and $[FeCl_4]^-$ anion, respectively (Table 3).

According performes calculations, the total energy is -33.5 kJ/mol. As it is shown in Table 3, the dispersion energy makes the maximum contribution to the total interaction energy and plays the main role in the formation of the π–π stacking in the crystal.

Table 3. Calculated π–π stacking energy (kJ/mol).

N	Symop	R	Electron density	E_ele	E_pol	E_dis	E_rep	E_tot
2	1 x, -y+1/2, z+1/2	4.05	B3LYP/6-31G(d,p)	20.5	-15.84	-73.39	35.23	-33.5

5. Conclusions

During the solution-assistance mechanochemical synthesis of ferrate chloride with methylene blue has been obtained a salt-type complex $[MB][FeCl_4]$. The crystal structure of the compound was determined by the single crystal X-ray diffraction method. The lanar $[MB]^+$ cations are stacked in an antiparallel fashion with the sulfur atom disposed alternatively on opposite sides. The centroid–centroid distances between stacked MB^+ cations vary from of 3.609 (2) to 3.802 (2) Å. Intermolecular interaction energy calculated for pair of the $[MB]^+$ cations is -33.5 kJ/mol. The energy of dispersion interaction exceeds the energies of repulsive interactions and is responsible for the formation of π-π stacks in the crystal structure.

Acknowledgments

The authors are grateful to their colleagues in the Institute of Bioorganic Chemistry of the Academy of Sciences of the Republic of Uzbekistan for supporting the X-ray experiment.

References

[1]. Kayabaşi, Y. & Erbaş, O. Methylene blue and its importance in medicine. *D. J. Med. Sci*. 2020, **6**, 136–145.
[2]. Oz, M., Lorke, D. E. & Petroianu, G. A. Methylene blue and Alzheimer's disease.

Biochemical Pharmacology. *Biochem Pharmacol.* 2009, **78**, 927–932.

[3]. Scigliano, G. & Scigliano, G. A. Methylene blue in covid-19. *Med. Hypotheses.* 2021, **146**, 110455–110470.

[4]. Rehman, H. U. Methemoglobinemia. *West J. Med*. 2001, **175**, 193–196.

[5]. Raj, M. M., Dharmaraja, A., Kavitha, S. J., Panchanatheswaran, K. & Lynch, D. E. Mercury(II)–methylene blue interactions: Complexation and metallate formation. *Inorg. Chim. Acta.* 2007, **360**, 1799–1808.

[6]. Pearson, R. G. Hard and soft acids and bases. *J. Am. Chem. Soc.* 1963, **85**, 3533–3539.

[7]. Canossa, S., Bacchi, A., Graiff, C., Pelagatti, P., Predieri, G., Ienco, A., Manca, G. & Mealli, C. Hierarchy of Supramolecular Arrangements and Building Blocks: Inverted Paradigm of Crystal Engineering in the Unprecedented Metal Coordination of Methylene Blue. *Inorg. Chem.* 2017, **56**, 3512–3516.

[8]. Sabirov V. Kh., Kadirova M. X. Crystal structure of three chloridocuprate(I, II) complexes with methylene blue (MB) counterions. *Z. Naturforsch*. B. 2022, https://doi.org/10.1515/znb-2022-0146.

[9]. CrysAlis Pro Software System (version 1.171.40.84a), Intelligent Data Collection and Processing Software for Small Molecule and Protein Crystallography, Rigaku Oxford Diffraction: Yarnton, Oxfordshire (U. K.), 2020.

[10]. Bourhis, L. J., Dolomanov, O. V., Gildea, R. J., Howard, J. A. K. & Puschmann, H. OLEX2: A Complete Structure Solution, Refinement and Analysis Program.*Acta Cryst.* 2015, A**71**, 59–75.

[11]. Sheldrick G. M. *Acta Crystallogr*. (2015). SHELXT-Integrated Space-Group and Crystal-Structure Determination. A71, 3.

[12]. Sheldrick, G. M. Crystallographic Computing. Ed. Moras D., Podjarny A. D., Thierry J. C. 1992, 145 - 157. IUCr. and OUP: Oxford, UK.

[13]. Macrae, C. F., Bruno, I. J., Chisholm, J. A., Edgington, P. R., McCabe, P., Pidcock, E., Rodriguez-Monge, L., Taylor, R., van de Streek, J. & Wood, P. A. New Features for the Visualization and Investigation of Crystal Structures.*J. Appl. Cryst.* 2008, **41**, 466–470.

[14]. Spek A. L. *PLATON* SQUEEZE: a tool for the calculation of the disordered solvent contribution to the calculated structure factors. *Acta Cryst*. 2009, D**65**, 148–155.

[15]. Spek A. L. Structure validation in chemical crystallography. *Acta Cryst*. 2015, C**71**, 9–18.

[16]. Spackman, M. A. & Byrom, P. G. A novel definition of a molecule in a crystal. *Chem. Phys. Lett.* 1997, **267**, 215–220.

[17]. Spackman, M. A. & McKinnon, J. J. Fingerprinting intermolecular interactions in molecular crystals. *CrystEngComm.* 2002, **4**, 378–392.

[18]. Spackman, P. R., Turner, M. J., McKinnon, J. J., Wolff, S. K., Grimwood, D. J., Jayatilaka, D. & Spackman, M. A. *CrystalExplorer*: a program for Hirshfeld surface analysis, visualization and quantitative analysis of molecular crystals. *J. Appl. Cryst*. 2021, 54, 1006–1011.

[19]. Canossa, S., Predieri, G. & Graiff, C. Hydrogen bonds and π-π Interactions in two new crystalline phases of methylene blue. *Acta Cryst.* 2018, E**74**, 587–593.

[20]. Groom, C. R., Bruno, I. J., Lightfoot, M. P. & Ward, S. C. The Cambridge Structural Database. *Acta Cryst.* 2016, B**72**, 171–179.

[21]. Marr, H., Stewart, J. M. & Chiu, M. F. The Crystal Structure of Methylene Blue. *Acta Cryst.* 1973, B**29**, 847-853.

[22]. Kavitha, S. J., Raj, M. M., Panchanatheswaran, K. & Lynch, D. E. 3, 7-Bis (dimethylamino) phenothiazin-5-ium nitrate dihydrate. *Acta Cryst.*2004, E**60, 60**, o1367–o1369.

[23]. Florence, Hg., Naorem, H. Dimerization of methylene blue in aqueous and mixed aqueous organic solvent: A spectroscopic study*J. Mol. Liquids.* 2014,198, 255–258.